2024 European Control Conference (ECC)
June 25-28, 2024. Stockholm, Sweden

The Role of Trajectory Planners in Lane Change Tracking Control: A Monte Carlo Evaluation of Four Controllers under Uncertainty

Markus Gurtner, Jakob Weber and Patrik Zips
Center for Vision, Automation & Control,
AIT Austrian Institute of Technology GmbH, Vienna, Austria
Email: markus.gurtner@ait.ac.at

Andreas Kugi
Automation and Control Institute, TU Wien, and
AIT Austrian Institute of Technology GmbH,
Vienna, Austria

***Abstract*— In the realm of autonomous transportation, executing vehicle manoeuvres accurately and reliably is paramount. The usual separation of trajectory planning and tracking, due to diverse origins and complexities, can lead to limitations in the closed-loop tracking behaviour. Nonlinear vehicle dynamics, stemming from nonholonomic constraints and tyre-road interactions demand simplified models for real-time planning.**

This paper comprehensively evaluates the combination of three trajectory planners with four tracking controllers using Monte Carlo analysis, considering scenario and model uncertainties. While planners use simplified or no models, tracking controllers based on nominal models can deviate due to uncertain parameters and environmental variations. Our study systematically evaluates tracking performance under uncertainty, supposing feasible planned trajectories adhering to physics-based constraints. We explore tracking error consistency across trajectory planners, assessing if feasibility alone can limit tracking errors.

I. INTRODUCTION

In autonomous transportation, the ability of vehicles to autonomously plan and execute manoeuvres with a high degree of accuracy and reliability is of utmost importance, and is approached in various directions [1, 2]. Historically, path or manoeuvre planning, execution, and trajectory tracking have often been treated as distinct topics. This is motivated by the pragmatic consideration that the components and algorithms involved may originate from diverse sources and encompass varied levels of complexity and abstraction. While this separation may seem prudent, it inherently harbours limitations that can undermine vehicle operations' overall effectiveness, accuracy, and reliability. Model predictive control approaches aim to bring planning and execution closer together, primarily relying on simplified vehicle dynamic models [3].

The complexity inherent to nonlinear vehicle dynamics, mainly due to the nonholonomic characteristics and the nonlinear interaction between the vehicle's tyres and the road surface [4] necessitates the utilization of simplified models to meet the real-time computational demands for manoeuvre planning. Consequently, planners frequently resort to simplified models, such as the kinematic bicycle model [5], a point mass model [3], or even use no model at all [6]. However, these assumptions can result in plans that do not align with the physical behaviour of the actual vehicle, highlighting the necessity of using refined models that encompass feasibility constraints. Addressing this issue requires the formulation of simplified models capable of integrating feasibility constraints, enabling the verification of trajectory limits throughout the planning phase. Noteworthy contributions, e.g., [7] and [8], have employed a constrained second-order model to successfully plan trajectories with a low computational footprint. More recently, [9] utilizes a kinematic bicycle model in an optimization-based planner with additional first principle feasibility checks that aim to approximate the tyre nonlinearity.

Nonetheless, even if a planned manoeuvre is feasible, ensuring minimal deviation of the vehicle movement from the plan remains a substantial challenge for the control algorithm. A remaining discrepancy can be attributed to uncertain model parameters that can cause the nominal planning model to diverge from the real vehicle. Furthermore, the performance of tracking controllers, which are often designed based on a nominal vehicle model, plays a significant role in determining tracking accuracy. Hence, variations in vehicle or environmental parameters persist as crucial factors influencing the tracking behaviour on a planned trajectory.

A substantial body of literature has emerged that evaluates the robustness of vehicle dynamic controllers, primarily focusing on maintaining stability and performance in the presence of perturbations and parameter variations. The tracking performance analysis for changed vehicle parameters is shown, e.g., in [10], where the vehicle mass and the cornering stiffness are varied, or in [11], where mass, rotational inertia, and center of gravity position are altered. The latter and [6] discuss also the influence of an initial deviation in vehicle position and orientation. A Monte Carlo based assessment of the influence of measurement noise is shown in [6] and [11]. An assessment of multiple discrete benchmark scenarios for model-based and model-free controllers is given in [12]. Recently, [13] presented a Monte Carlo simulation toolbox for uncertainty quantification of closed-loop systems, which provides a solver for stochastic differential equations (SDEs) and thus enables a straightforward assessment of stochastic disturbances or uncertainties. For assessing the tracking performance resulting from a worst-case sequence of measurement errors, [6] proposed the use of Rapidly-exploring Random Trees (RRT), also applied in [11]. A formal approach to verify a planned trajectory is shown in [14], where the dynamic system is linearised to efficiently

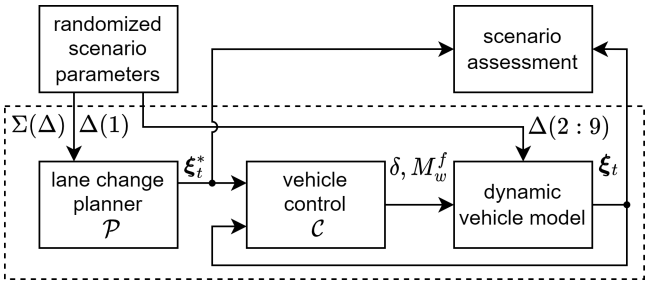

Fig. 1. Configuration for the assessment of a highway lane change manoeuvre with varying planner $\mathcal{P}$ and controller $\mathcal{C}$ combinations where the overall system Σ is subject to a randomized configuration vector Δ.

perform a reachability analysis and determine all reachable positions. However, a noteworthy limitation of the discussed evaluations lies in their semi-static nature — manoeuvre scenarios usually remain fixed, rendering the approaches unsuitable for addressing real-world driving dynamics and online manoeuvre planning.

Our contribution goes beyond evaluations for static or discrete manoeuvres by considering scenario and model parameter variations within the analysis. Bridging trajectory planning and tracking control, our research illuminates the interplay between planner and tracking accuracy on a representative subset of planners and controllers. Specifically, the study seeks to determine whether the closed-loop tracking performance changes when the trajectory planner itself is varied. Moreover, the research aims to discern whether the requirement of planned trajectory feasibility alone suffices to limit tracking errors or if additional requirements are imperative.

II. METHODOLOGY

In the scope of this contribution, we analyse the tracking performance of different controllers during a highway lane change. Specifically, it is interesting whether and how the used planning algorithm influences the tracking performance of the overall closed-loop system. For a rigorous assessment, nominal behaviour, scenario variations, and measurement errors will be considered. A block diagram illustrating the chosen approach is given in Fig. 1.

This section begins with an introduction to established planning algorithms $\mathcal{P}_i$, followed by suitable vehicle dynamics controllers $\mathcal{C}_i$, a subset of the countless implementations in the literature [2]. Next, a dynamic vehicle model is discussed briefly, based on which the considered scenario variations, parameter uncertainties, and measurement errors are introduced. At the end of this section, the Monte Carlo-based approach for assessing the closed-loop tracking performance is motivated.

A. Lane Change Trajectory Planners

As a highway lane change is discussed, all planners will use a fixed lane width $l_{lw} = 3.5\,\mathrm{m}$. The nominal longitudinal velocity is $v_l = 100\,\mathrm{km\,h^{-1}}$, and the lane change time T_{lc} will vary from $2.5\,\mathrm{s}$ to $4.5\,\mathrm{s}$, representing a range from fast to slow manoeuvre [15]. Obstacle detection and decision-making can be omitted, as the tracking performance on the planned trajectories is analysed.

TABLE I

OVERVIEW OF ANALYSED PLANNERS AND CONTROLLERS.

Planners	**Controllers**
$\mathcal{P}_a$ State variable filter	$\mathcal{C}_a$ Flatness-based FF & PD control
$\mathcal{P}_b$ 5th order polynomial	$\mathcal{C}_b$ Exact input/output linearisation
$\mathcal{P}_c$ Dynamic optimization on kinematic single-track model	$\mathcal{C}_c$ Higher-order sliding mode
	$\mathcal{C}_d$ Immersion & Invariance principle

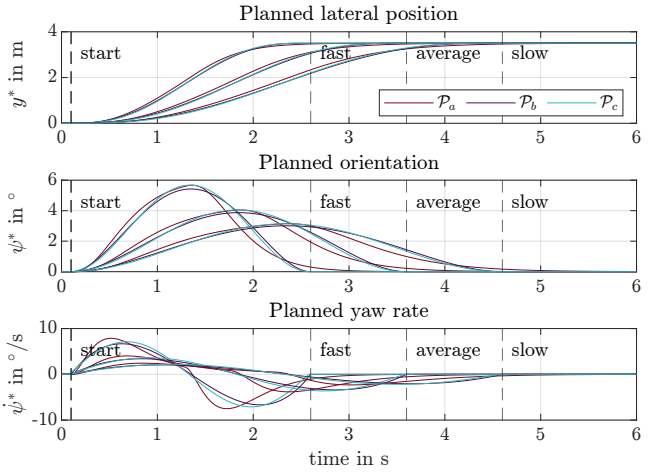

Fig. 2. Planned lane change trajectories for three manoeuvre speeds with three different planners.

In this contribution, the simplest planner $\mathcal{P}_a$ uses a filter-based approach to determine an appropriate trajectory for the lane change. Specifically, a state variable filter (SVF) with a lane change dependent filter time $T_f = T_{lc}/15$ and a preceding rate limiter for the lateral set point with $2.2 l_{lw}/T_{lc}$ is used[1]. The second planner $\mathcal{P}_b$ constructs a 5th order polynomial for the lateral position, see [16]. Thereby, start and end conditions for determining the polynomial coefficients are uniquely defined by the lane change manoeuvre itself. Finally, the third planner $\mathcal{P}_c$ is a model-based planner. Here, a dynamic optimization problem with fixed initial and terminal values is formulated, where the solution must respect the dynamics of the kinematic single-track model while minimizing steering and accelerating action, see [5, 9]. As a summary, the planners are listed in Tab. I.

All selected planners provide desired values for the longitudinal quantities $\boldsymbol{\xi}_l^* = (x^*, v_l^*, a_l^*)$, with the longitudinal position x, the longitudinal velocity v_l and the longitudinal acceleration a_l, and the lateral dynamic quantities $\boldsymbol{\xi}_t^* = \left(y^*, \psi^*, \dot{\psi}^*\right)$, with the lateral position y, the orientation ψ and the yaw rate $\dot{\psi}$, respectively. As the longitudinal velocity remains nearly constant during a highway lane change, the comparison of the three planning approaches and all further parts of this analysis will focus solely on the lateral quantities

[1]Note that this planner is tuned empirically to provide trajectories rather similar to the other planners.

$\boldsymbol{\xi}_t^*$. Fig. 2 illustrates the planned lateral position y^*, planned orientation ψ^*, and planned yaw rate $\dot{\psi}^*$ for the three planners for fast ($T_{lc} = 2.5\,\mathrm{s}$), average ($T_{lc} = 3.5\,\mathrm{s}$), and slow ($T_{lc} = 4.5\,\mathrm{s}$) lane changes.

B. Vehicle Dynamics Controllers

To track the planned trajectories, four different tracking controllers will be utilized. These controllers are also a subset of the comparison performed in [11], allowing us to compare our results. It can be noticed that each controller is based on a different control approach and relies on a different amount of a priori knowledge w.r.t. the vehicle.

The first controller $\mathcal{C}_a$ uses the flatness property of the kinematic bicycle model to calculate an idealized steering angle and the acceleration as a feedforward (FF) component. The actual tracking is realized by PD feedback control, see [14]. Note that the model-free PD controller is not re-tuned to fit the considered vehicle, which will cause significant performance degradation. Second, $\mathcal{C}_b$ performs exact input/output linearisation on a single-track model with nonlinear tyre forces [6]. Specifically, this control requires a nominal model for the lateral tyre forces. Next, $\mathcal{C}_c$ is a higher-order sliding mode controller using the super-twisting algorithm, as discussed in [10]. As a model-based approach, the controller is designed for a single-track model with linearised tyre characteristics. The fourth and last controller $\mathcal{C}_d$ can also be found in [10] and is based on the Immersion & Invariance principle. Again, a single-track model with linear tyre characteristics acts as a design model. As a summary, the controllers are listed in Tab. I.

C. Dynamic Vehicle Model

For the simulation study, the vehicle dynamics are formulated for a single-track model in the vehicle fixed reference frame, see [17]. The longitudinal acceleration a_l and the lateral acceleration a_t are modelled by

$$m a_l = F_l^r + F_l^{ext} + \cos(\delta)\, F_l^f - \sin(\delta)\, F_t^f \tag{1}$$
$$m a_t = F_t^r + F_t^{ext} + \sin(\delta)\, F_l^f + \cos(\delta)\, F_t^f, \tag{2}$$

with the vehicle mass m, the steering angle δ, the longitudinal and lateral tyre forces $F_{\{l,t\}}^{\cdots}$ on the front and rear axle $F_{\cdots}^{\{f,r\}}$, and the external forces $F_{\cdots}^{ext}$ acting on the centre of gravity[2]. The dynamics of the orientation ψ are modelled by

$$J_\psi \ddot{\psi} = l_f \left(F_t^f \cos(\delta) + F_l^f \sin(\delta) \right) - l_r F_t^r + M_\psi^{ext}, \tag{3}$$

with the yaw moment of inertia J_ψ, the front and rear axle distance to the centre of gravity (COG) l_f and l_r. and an external yaw moment M_ψ^{ext}. Due to the vehicle fixed reference frame, kinematic couplings need to be considered

$$a_t = \dot{v}_t + v_l \dot{\psi} \qquad \text{and} \qquad a_l = \dot{v}_l - v_t \dot{\psi} \tag{4}$$

to determine the time derivatives of the vehicle fixed velocities v_l and v_t. The output trajectory of the vehicle in road coordinates is given by

$$\dot{x} = v_l \cos(\psi) - v_t \sin(\psi) \tag{5}$$
$$\dot{y} = v_l \sin(\psi) + v_t \cos(\psi). \tag{6}$$

The lateral tyre forces F_t^f and F_t^r in (1)–(3) are modelled by Pacejka's well known magic tyre formula

$$F_\alpha = F_z \mu_r \sin(C \operatorname{atan}(B\alpha(1-E) + E \operatorname{atan}(B\alpha))), \tag{7}$$
$$F_t^f = -F_\alpha^f, \qquad F_t^r = -F_\alpha^r, \tag{8}$$

with the tyre parameters B, C, E, and the road friction coefficient μ_r, see [4]. The front and rear tyre loads F_z^f and F_z^r are modelled via a static load distribution according to

$$F_z^f = mg \frac{l_r}{l_f + l_r}, \qquad F_z^r = mg \frac{l_f}{l_f + l_r}, \tag{9}$$

and the tyre slip angles for the front and rear tyre α^f and α^r are

$$\alpha^f = \operatorname{atan}\left(\frac{v_t + l_f \dot{\psi}}{|v_l|} \right) - \delta \tag{10}$$
$$\alpha^r = \operatorname{atan}\left(\frac{v_t - l_r \dot{\psi}}{|v_l|} \right). \tag{11}$$

As a highway lane change without distinct acceleration or deceleration is considered, the longitudinal tyre forces are modelled as

$$F_l^r = -F_z^r c_{fr}, \qquad F_l^f = -F_z^f c_{fr} + \frac{M_w^f}{r_t}, \tag{12}$$

with the tyre friction loss coefficient c_{fr}, the dynamic tyre radius r_t, and the motor torque on the front wheel M_w^f.

The nominal model parameters are given in Tab. II and are based on the Mercedes Benz C220 parameter set from [18].

TABLE II
NOMINAL PARAMETERS FOR THE DYNAMIC VEHICLE MODEL.

Symbol	Description	Value	Unit
m	Total vehicle mass	1654	kg
g	Gravitational acceleration	9.81	$\mathrm{m\,s^{-2}}$
J_ψ	Jaw moment of inertia	2200	$\mathrm{kg\,m\,s^{-2}}$
l_f	Front axle distance to COG	1.34	m
l_r	Rear axle distance to COG	1.42	m
μ_r	Road friction coefficient	0.9	-
B	Magic formula stiffness factor	10	-
C	Magic formula shape factor	1.3	-
E	Magic formula curvature factor	-0.25	-
c_{fr}	Tyre friction coefficient	0.013	-
r_t	Dynamic tyre radius	0.303	m

D. Scenario and Model Parameter Variations

When analysing the influence of varying scenarios and model parameters for closed-loop systems, it is always important to determine reasonable parameter ranges. As already discussed in Sec. II-A, the lane change time will be varied from $2.5\,\mathrm{s}$ to $4.5\,\mathrm{s}$, representing the range from fast to slow manoeuvres [15].

[2]External forces can incorporate air drag or head winds.

TABLE III

CONSIDERED SCENARIO AND PARAMETER VARIATIONS.

Parameter		Min.	Max.	Unit
Planner / Scenario				
T_{lc}	Lane change time	2.5	4.5	s
Vehicle parameters				
Δm	Additional mass	0	500	kg
Δl	Position of additional mass	-0.28	0.28	m
B	Magic formula stiffness factor	8	12	-
C	Magic formula shape factor	1.1	1.4	-
E	Magic formula curvature factor	-10	0	-
μ_r	Road friction coefficient	0.7	1	-
Initialization				
ε_y	Lateral deviation	-0.1	0.1	m
ε_ψ	Orientation deviation	-0.5	0.5	°

Besides the scenario configuration, additional variations will be considered. Therefore, an additional mass Δm is introduced, which is placed at a distance Δl in front of the centre of gravity of the bicycle model. This leads to an increased vehicle mass m' and yaw moment of inertia J'_ψ according to

$$m' = m + \Delta m \quad \text{and} \quad J'_\psi = J_\psi + \Delta l^2 \Delta m. \tag{13}$$

Furthermore, the mass shifts the centre of gravity, resulting in the new front and rear axle distances l'_f and l'_r as

$$l'_f = l_f - \frac{\Delta l \Delta m}{m'} \quad \text{and} \quad l'_r = l_r + \frac{\Delta l \Delta m}{m'}. \tag{14}$$

Adjusted vertical tyre loads are calculated according to (9).

For considering varying road conditions, the road friction coefficient μ_r will be varied from 0.7 to 1.0, representing dry road conditions. As the main contact point between the vehicle and the road, the tyre model significantly influences the vehicle dynamics. The tyre model parameter ranges result from the discussed parameter variations in [4].

As trajectory planning, especially re-planning, relies on accurate information about the current vehicle state and position, it is crucial to investigate the influence of errors in the odometric information. Focusing on a lane change, initial errors in the lateral position and the orientation according to [6] will be assumed in the scope of this contribution. These kinds of offsets can be introduced, e.g., via an initial model state $y|_{t=0} = \varepsilon_y$ and $\psi|_{t=0} = \varepsilon_\psi$.

To obtain a compact notation, the discussed scenario parameters, model parameters, and error ranges are summarized according to

$$\Delta = \{T_{lc}, \Delta m, \Delta l, B, C, E, \mu_r, \varepsilon_y, \varepsilon_\psi\}, \quad \Delta \in \mathcal{B}_\Delta, \tag{15}$$

where $\mathcal{B}_\Delta$ is specified according to Tab. III.

E. Monte Carlo based Performance Assessment

Considering only corner cases for $\dim(\mathcal{B}_\Delta) = 9$ would already require $2^9 = 512$ simulations for assessing the performance of the closed-loop system while still omitting samples in the parameter space $\mathcal{B}_\Delta$. Improved coverage with an additional central case would lead to $3^9 = 19683$ simulations. Therefore, a Monte Carlo based performance assessment with $N_{mc} = 5000$ is performed as a more efficient alternative to a grid-based assessment [19].

For the probabilistic performance assessment of the closed-loop system, a performance metric must be specified. As the lane change is in focus, it is evident that the lateral tracking error $e_y = y - y^*$ and the orientation error $e_\psi = \psi - \psi^*$ will be of special interest. When assessing the performance via a Monte Carlo approach, see [20], it is beneficial to assess each scenario with a low-dimensional quantity. Therefore, and based on our prior work [21], the maximum of the absolute errors up to a simulation time $T_E = 6\,\mathrm{s}$ according to

$$\bar{\gamma}_i = \max_{\forall \tau \in [0, T_E]} |e_i(\tau)| \quad \text{with} \quad i \in \{y, \psi\} \tag{16}$$

will serve as a performance function for the closed-loop behaviour.

The performance of each planner and controller combination can then be compared by analysing the distribution of the respective statistics. After generating N_{mc} randomized scenario configurations $\Delta_k \in \mathcal{B}_\Delta$, $k = 1, ..., N_{mc}$, the statistics of the performance metrics $\bar{\gamma}_{i,k}$ can be compared, e.g., by investigating the empiric distribution functions, by gathering the data in histograms, or by analysing the empirical worst-case performance $\bar{\gamma}_i^{wc} = \max_k(\bar{\gamma}_{i,k})$.

III. EXPERIMENTAL STUDY

The conducted experiments consist of three stages. First, the planners and controllers under test are assessed on the nominal vehicle model. The generated trajectories are first verified with physics-based feasibility checks to indicate the expected closed-loop performances. Second, the influence of scenario and vehicle parameter variations will be investigated using the Monte Carlo based approach. Third, additional initial offsets are introduced at planned manoeuvres beginning.

A. Nominal Assessment and Physics-based Feasibility Checks

Typically, vehicles cannot follow all arbitrary trajectories. On the one hand, this is due to the rigid rear axle, which leads to nonholonomic vehicle models. On the other hand, the force that the tyres can transfer to the road is limited. In the first step, we will check if the planned trajectories fulfil these constraints. Therefore, the kinematic bicycle model will be used. In [9], three feasibility constraints are discussed. The longitudinal velocity constraint can be omitted here, as the manoeuvre velocity is fixed. The maximum acceleration $\bar{a}$ is determined by the tyre-road friction coefficient μ_r and the gravitational acceleration g according to

$$a_l^2 + a_t^2 \leq \bar{a}^2, \quad \text{with} \quad \bar{a} = \mu_r g. \tag{17}$$

Assuming a low friction coefficient $\mu_r = 0.7$ yields $\bar{a} \approx 6.87\,\mathrm{m\,s^{-2}}$ as lower estimate for the maximum acceleration. Again, the longitudinal acceleration a_l is neglected due to a nearly constant velocity. Assuming constant velocities, the planned lateral acceleration can be calculated with the

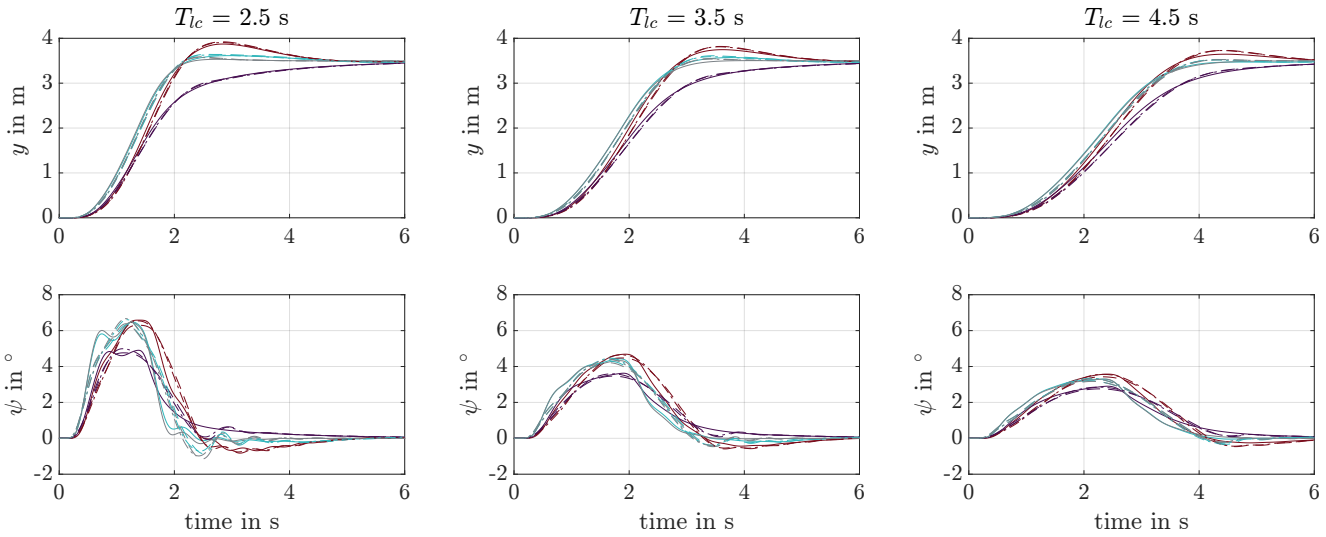

Fig. 3. Simulated tracking performance with varying planners (line style) and controllers (colour) with the nominal vehicle model.

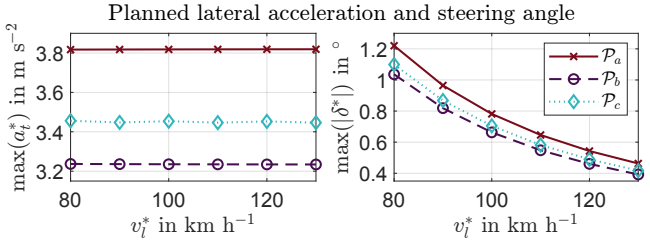

Fig. 4. Planned lateral acceleration a_t^* and steering angle δ^* for the fast lane change ($T_{lc} = 2.5\,\mathrm{s}$) with varying longitudinal speed v_l^* and all three planners.

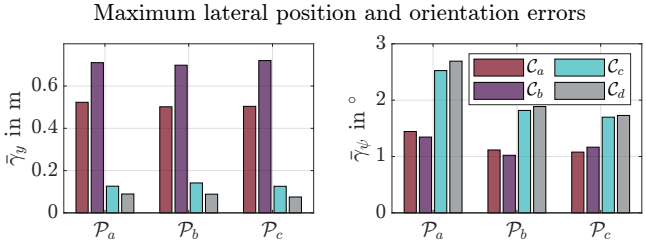

Fig. 5. Simulated maximum tracking errors with varying planners (groups) and controllers (colour) with the nominal vehicle model for the fast lane change ($T_{lc} = 2.5\,\mathrm{s}$).

planned yaw rate $\dot{\psi}^*$ and the longitudinal velocity v_l^* according to (4) as

$$a_t^* = \dot{\psi}^* v_l^*. \tag{18}$$

The calculated maximum acceleration for each planner at varying velocities are given in the left part of Fig. 4. It can be seen that all planners yield trajectories with accelerations far below the discussed limit. Also relevant is the limitation in the steering angle, which is a constructive parameter. For the considered vehicle, the steering angle is constrained to $|\delta| \leq 20°$. Using the yaw dynamics according to the kinematic bicycle model

$$\dot{\psi} = \frac{v_l}{l_r + l_f} \tan(\delta), \tag{19}$$

see e.g., [5, 9], leads directly to the planned steering angle

$$\delta^* = \operatorname{atan}\left(\frac{\dot{\psi}^*}{v_l^*}(l_r + l_f)\right). \tag{20}$$

The maximum values for each planner at different velocities are again shown in the right part of Fig. 4. As expected, for a highway manoeuvre, all planners come with planned steering angles below the discussed limit. Therefore, the physics-based checks indicate per se feasible planning results.

In addition, Fig. 3 shows the tracking behaviour for all possible combinations of planners (line styles) and controllers (colours) for fast, average, and slow lane changes. All lane changes are planned for $v_l^* = 100\,\mathrm{km\,h^{-1}}$, and the simulations are performed on the nominal vehicle model without any additional sources of uncertainty or errors. The top row shows the simulated lateral position y, and the bottom row depicts the simulated orientation ψ. Especially for the fast lane changes, some oscillations in the orientation become visible for some combinations. Nevertheless, these oscillations do not influence the lateral tracking significantly. Together with Fig. 5, it is clearly visible that the choice of the controller dominates the tracking performance. The choice of the planner seems less relevant, at least for the nominal scenarios. When focusing on the tracking performance for y, the controllers $\mathcal{C}_c$ and $\mathcal{C}_d$ are performing better than $\mathcal{C}_a$ and $\mathcal{C}_b$, while the choice of the planner is barely noticeable. For the orientation ψ, $\mathcal{C}_a$ and $\mathcal{C}_b$ show an advantage against $\mathcal{C}_c$ and $\mathcal{C}_d$, while all controllers perform worse with planner $\mathcal{P}_a$.

B. Scenario and Model Parameter Variations

Next, parameter variations in the scenario and the dynamic vehicle model are investigated by applying a Monte Carlo scheme. Therefore, $N_{mc} = 5000$ randomized parameter vectors $\Delta_k \in \mathcal{B}_\Delta$ are sampled using a uniform distribution and random sampling, see (15). The initial offsets are set to

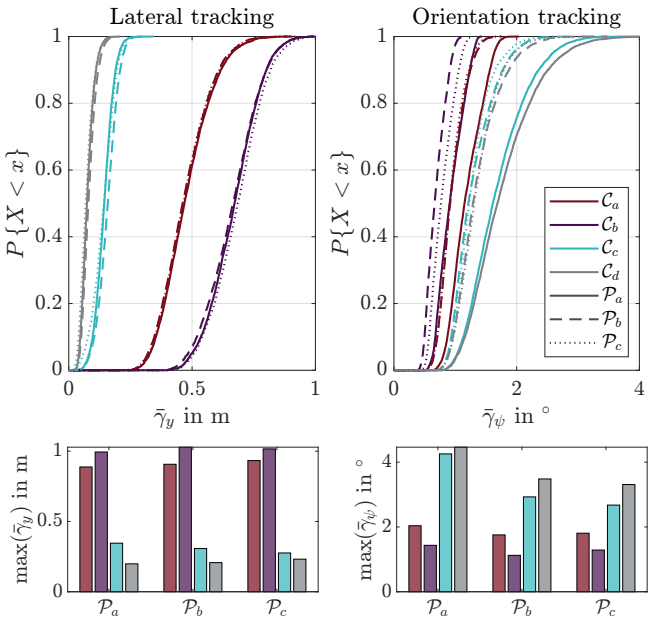

Fig. 6. Empirical distribution functions (top) and worst-case observations (bottom) for the tracking performance metrics under scenario and model parameter variations. Colours represent different controllers, while line styles denote varying planners.

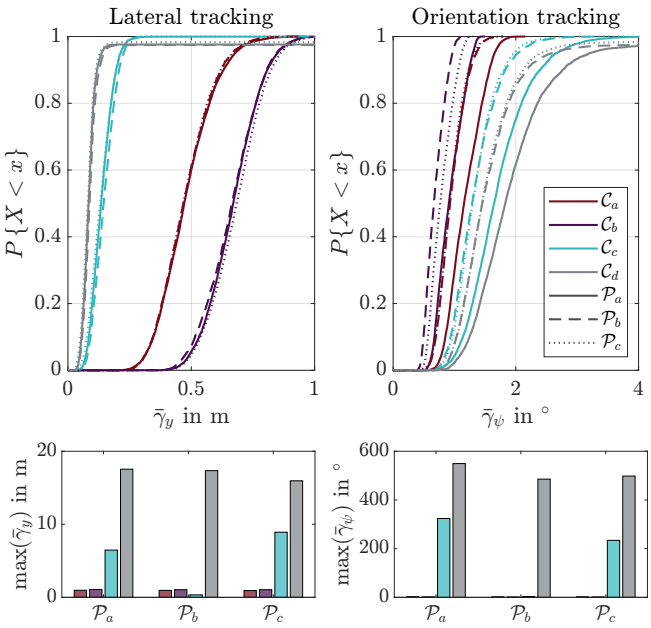

Fig. 7. Empirical distribution functions (bottom) and worst-case observations (bottom) for the tracking performance metrics with additional initial deviation. Colours represent different controllers, while line styles denote varying planners.

zero, $\varepsilon_y = 0$, $\varepsilon_\psi = 0$. Each sample Δ_k yields the closed-loop performance measures $\bar{\gamma}_{y,k}$ and $\bar{\gamma}_{\psi,k}$ for each pair of planner and controller. Using the results of these simulations, Fig. 6 shows the determined empirical distribution functions (EDF) for each planner (line style) and controller (colour) combination in the top part and the observed worst-case performance in the bottom part. The upper representation is beneficial for an assessment of the closed-loop performance, since it is directly visible which share of the tested configurations meets a specific performance limit. The further to the left in the plot the EDF is found, the lower the expected errors are. The empirical worst-case performance is given as additional information in the bottom part.

Like Fig. 3, controller $\mathcal{C}_d$ has the best tracking performance in $\bar{\gamma}_y$. With all controllers, hardly any influence of the used planners is visible in $\bar{\gamma}_y$, neither in the EDFs nor in the worst-case representation. In contrast, the orientation metric $\bar{\gamma}_\psi$ significantly depends on the selected planner. Using the planner $\mathcal{P}_a$ consistently leads to a worse performance as the EDFs are shifted towards higher tracking errors. Particularly, an increase in the empirical worst-case performance can be observed for the controllers $\mathcal{C}_a$ and $\mathcal{C}_b$.

It appears that using $\mathcal{C}_c$ together with $\mathcal{P}_c$ provides a good trade-off between lateral position and orientation tracking.

C. Manoeuvre Initialisation with Deviation

As a final step, all parameter variations and initial deviations according to Tab. III are considered in the assessment of the lane change manoeuvre. Again, the EDFs for all planner (line style) and controller (colour) combinations are depicted in Fig. 7 (top) and the empiric worst-case performance values in Fig. 7 (bottom). For comparability, the axis limits are identical to Fig. 6, even though some planner and controller combinations lead to EDFs that significantly exceed these limits.

The overall interpretation of the EDFs is consistent with the prior section, where the variations in $\bar{\gamma}_y$ are dominated by the selected controller and the degradation by choosing $\mathcal{P}_a$ is evident in $\bar{\gamma}_\psi$. It is much more revealing to analyse the empirical worst-case performances. Interestingly, the controller $\mathcal{C}_d$, which previously performed best on $\bar{\gamma}_y$, now has the worst empirical worst-case performance. In contrast, the controllers $\mathcal{C}_a$ and $\mathcal{C}_b$ are less sensitive to the introduced deviations in the manoeuvre initialisation. With controller $\mathcal{C}_d$, worst-case performances of $\bar{\gamma}_\psi > 180°$ are observed for all planners. This indicates a skidding vehicle and therefore, a failure of the closed-loop control system. An interesting result is that the controller $\mathcal{C}_c$, together with the planner $\mathcal{P}_b$, exhibits the best tracking behaviour. However, the combination with the other planners $\mathcal{P}_a$ and $\mathcal{P}_c$ also leads to large errors. In order to assess the reliability of these empirical estimates, the sample size bound for the worst-case performance is utilized, e.g., [20, 21]. Demanding a confidence parameter $\beta = 10^{-3}$ yields $\epsilon = 1 - \beta^{N_{mc}^{-1}} \approx 1.381 \cdot 10^{-3}$ as bound for an even worse performance on a new sample Δ_{k+1}, i. e.,

$$\Pr\left\{\Pr\left\{\max_k(\bar{\gamma}_{i,k}) < \bar{\gamma}_{i,k+1}\right\} < \epsilon\right\} \geq 1 - \beta. \qquad (21)$$

Given the considered variations according to Tab. III and the carried out simulations, Fig. 7 strongly indicates that within the analysed planner and controller combinations, the pair $\mathcal{P}_b$ and $\mathcal{C}_c$ works best.

IV. CONCLUSIONS

This study culminates in several key findings that provide insight into the interplay between trajectory planning and tracking control for autonomous vehicles under uncertainty. Our evaluation demonstrates that all analysed planners generate physically feasible trajectories for the tested lane change times and speeds. When only varying vehicle parameters, our results reveal that all tracking controllers can successfully follow the trajectories generated by the planners. However, controllers $\mathcal{C}_a$ and $\mathcal{C}_b$ show substantial deviations even under nominal conditions, indicating limitations in their control performance. Importantly, incorporating initial errors into the analysis uncovers the inability of some controllers to maintain tracking. This highlights that while certain controllers might perform well under ideal conditions, their robustness diminishes when faced with deviations from the nominal model. Individual pairs of planners and controllers are influenced in varying degrees, with the combination of $\mathcal{P}_b$ and $\mathcal{C}_c$ performing best in the considered scenarios. Overall, the controller selection notably influences tracking errors the most. Nonetheless, it becomes evident that planner $\mathcal{P}_a$ consistently leads to larger deviations, particularly in vehicle orientation. This underscores the critical role of both planning and control components in achieving accurate and reliable trajectory execution.

These findings collectively underscore the complexity of achieving precise trajectory tracking in the presence of uncertainties. As the autonomous driving landscape continues to evolve, the symbiotic relationship between trajectory planning and tracking control necessitates careful consideration to ensure the robust and dependable operation of autonomous vehicles in real-world scenarios. It is also expected that the detailed analysis of the interplay between trajectory planning and tracking control is beneficial for general control systems besides the vehicle dynamics domain.

OPEN SCIENCE

We encourage the transformation towards an open science community. Therefore, our generated data, together with the relevant code for the analysis, is available under DOI 10.5281/zenodo.8402997.

ACKNOWLEDGMENT

The research leading to these results has received funding from the Mobility of the Future programme (Grant No. 884344). Mobility of the Future is a research, technology and innovation funding programme of the Republic of Austria, Ministry of Climate Action. The Austrian Research Promotion Agency (FFG) has been authorised for the programme management.

REFERENCES

[1] Y. Kebbati, N. Ait-Oufroukh, D. Ichalal, and V. Vigneron, "Lateral control for autonomous wheeled vehicles: A technical review," *Asian Journal of Control*, vol. 25, no. 4, pp. 2539–2563, 2023.

[2] W. Liu, M. Hua, Z. Deng, Z. Meng, Y. Huang, C. Hu, S. Song, L. Gao, C. Liu, B. Shuai, A. Khajepour, L. Xiong, and X. Xia, "A Systematic Survey of Control Techniques and Applications in Connected and Automated Vehicles," *IEEE Internet of Things Journal*, vol. 10, no. 24, pp. 21 892–21 916, 2023.

[3] N. A. Nguyen, D. Moser, P. Schrangl, L. del Re, and S. Jones, "Autonomous overtaking using stochastic model predictive control," in Proc. of *2017 11th Asian Control Conference (ASCC)*. Gold Coast, QLD, Australia: IEEE, 2017, pp. 1005–1010.

[4] H. B. Pacejka, *Tyre and Vehicle Dynamics*, 2nd ed. Amsterdam: Elsevier/BH, 2006.

[5] P. Zips, M. Böck, and A. Kugi, "Optimisation based path planning for car parking in narrow environments," *Robotics and Autonomous Systems*, vol. 79, pp. 1–11, 2016.

[6] D. Heß, M. Althoff, and T. Sattel, "Comparison of trajectory tracking controllers for emergency situations," in Proc. of *2013 IEEE Intelligent Vehicles Symposium (IV)*. Gold Coast, QLD, Australia: IEEE, 2013, pp. 163–170.

[7] F. Altché, P. Polack, and A. de La Fortelle, "High-speed trajectory planning for autonomous vehicles using a simple dynamic model," in Proc. of *2017 IEEE 20th International Conference on Intelligent Transportation Systems (ITSC)*. Yokohama, Japan: IEEE, 2017, pp. 1–7.

[8] M. Montani, L. Ronchi, R. Capitani, and C. Annicchiarico, "A Hierarchical Autonomous Driver for a Racing Car: Real-Time Planning and Tracking of the Trajectory," *Energies*, vol. 14, no. 19, 2021.

[9] Z. Han, Y. Wu, T. Li, L. Zhang, L. Pei, L. Xu, C. Li, C. Ma, C. Xu, S. Shen, and F. Gao, "An Efficient Spatial-Temporal Trajectory Planner for Autonomous Vehicles in Unstructured Environments," *arXiv preprint arXiv:2208.13160v2[cs.RO]*, 2022.

[10] G. Tagne, R. Talj, and A. Charara, "Design and Comparison of Robust Nonlinear Controllers for the Lateral Dynamics of Intelligent Vehicles," *IEEE Transactions on Intelligent Transportation Systems*, vol. 17, no. 3, pp. 796–809, 2016.

[11] D. Calzolari, B. Schurmann, and M. Althoff, "Comparison of trajectory tracking controllers for autonomous vehicles," in Proc. of *2017 IEEE 20th International Conference on Intelligent Transportation Systems (ITSC)*. Yokohama, Japan: IEEE, 2017, pp. 1–8.

[12] A. Artuñedo, M. Moreno-Gonzalez, and J. Villagra, "Lateral control for autonomous vehicles: A comparative evaluation," *Annual Reviews in Control*, vol. 57, p. 100910, 2024.

[13] M. R. Wahlgreen, A. Thode Reenberg, M. K. Nielsen, A. Rydahl, T. K. S. Ritschel, B. Dammann, and J. B. Jørgensen, "A High-Performance Monte Carlo Simulation Toolbox for Uncertainty Quantification of Closed-loop Systems," in Proc. of *2021 60th IEEE Conference on Decision and Control (CDC)*. Austin, TX, USA: IEEE, 2021, pp. 6755–6761.

[14] M. Althoff and J. M. Dolan, "Online Verification of Automated Road Vehicles Using Reachability Analysis," *IEEE Transactions on Robotics*, vol. 30, no. 4, pp. 903–918, 2014.

[15] A. Sporrer, G. Prell, J. Buck, and S. Schaible, "Realsimulation von Spurwechselvorgängen im Straßenverkehr," *VKU Verkehrsunfall und Fahrzeugtechnik*, vol. 36, no. 3, pp. 69–76, 1998.

[16] A. Mehmood, M. Liaquat, A. I. Bhatti, and E. Rasool, "Trajectory Planning and Control for Lane-Change of Autonomous Vehicle," in Proc. of *2019 5th International Conference on Control, Automation and Robotics (ICCAR)*. Beijing, China: IEEE, 2019, pp. 331–335.

[17] D. Ammon, *Modellbildung und Systementwicklung in der Fahrzeugdynamik*, ser. Leitfäden der angewandten Mathematik und Mechanik. Wiesbaden and Stuttgart: Springer and Teubner, 1997, vol. 73.

[18] M. Kamelreiter, *Fahrwerksregelung basierend auf kontinuierlichen und digitalen elektrorheologischen Dämpfern*, ser. Modellierung und Regelung komplexer dynamischer Systeme. Aachen: Shaker, 2012, vol. 15.

[19] J. Bergstra and Y. Bengio, "Random Search for Hyper-Parameter Optimization," *Journal of Machine Learning Research*, vol. 13, no. 10, pp. 281–305, 2012.

[20] R. Tempo, G. Calafiore, and F. Dabbene, *Randomized Algorithms for Analysis and Control of Uncertain Systems: With Applications*, 2nd ed. Springer, 2013.

[21] M. Gurtner, P. Zips, A. Trachte, and A. Kugi, "Application of Monte Carlo Method for Probabilistic Robust Control Performance Assessment," in Proc. of *2022 6th International Conference on System Reliability and Safety (ICSRS)*. Venice, Italy: IEEE, 2022, pp. 163–168.